# LIDAR SCAN MATCHING WITH RTK-GNSS POSITIONING AND GEOMETRIC CONSTRAINTS

Masafumi Nakagawa (1), Shinjiro Abe (1) , Sho Sanuka (1), Kazuo Saito (2) , Masahiro Miyo (3)

[1] Shibaura Institute of Technology, 3-7-5, Toyosu, Koto-ku, Tokyo, 135-8548, Japan
[2] EAMS ROBOTICS Co., Ltd., 2-21, Nishi-chuo, Fukushima city, Fukushima, 960-8074, Japan
[3] Watanabe Engineering Co., Ltd., 7-4-69, Noda-machi, Fukushima city, Fukushima, 960-8055, Japan
Email: mnaka@shibaura-it.ac.jp

**KEY WORDS:** Scan matching, Multilayer LiDAR, RTK-GNSS, Mobile mapping, Geometric constraints

**ABSTRACT:** Scan matching in simultaneous localization and mapping (SLAM) has several technical issues, such as error accumulation, high processing cost in point cloud matching and optimization, and position loss problems after scan matching failures. Error adjustment processing can improve the performance of SLAM with loop closure and global optimization approach. However, measurement path plans and higher processing cost are required for the error adjustment and global optimization. In contrast, global navigation satellite system (GNSS) positioning can simplify the scan matching. Thus, we propose scan matching for multilayer LiDAR data registration with RTK-GNSS positioning and geometric constraints. Through experiments on point cloud acquisition with multilayer LiDAR and a single-frequency RTK-GNSS positioning device, we verify that our methodology can integrate point clouds acquired in mobile mapping without an inertial measurement unit. We also confirm that our methodology can avoid error accumulation problems in conventional SLAM processing.

## 1. INTRODUCTION

The mobile three-dimensional (3D) measurement system is a measurement device used to acquire point clouds over a wide area with image acquisition and laser scanning while moving. Mobile 3D measurement systems can be mainly classified into camera-based systems and LiDAR-based systems. In this research, we focus on LiDAR-based systems.

Point cloud acquisition with a mobile 3D measurement system is processed with two steps. First, distance measurement results are acquired with LiDAR. Next, local point clouds are obtained with scanning angles on the scanner coordinates. Then, global point clouds are obtained based on the real-world coordinates of the LiDAR position and rotation data. The LiDAR position data are generally acquired with a total station-based position tracker or kinematic global navigation satellite system (GNSS) positioning device mounted on a mobile 3D measurement system. The rotation data of LiDAR are generally acquired with an inertial measurement unit (IMU) or multiple GNSS antennas. The mobile 3D measurement system in surveying fields consists of a GNSS positioning device, IMUs, and LiDAR. Moreover, wheel odometry is generally added to mobile 3D measurement systems to support IMUs for position data acquisition in poor satellite-based positioning environments. The absolute accuracy of point clouds acquired with mobile 3D measurement systems greatly depends on the performance of positioning devices. Moreover, the relative measurement accuracy, such as shape representation accuracy, of acquired point clouds greatly depends on the performance of IMUs. In outdoor environments, kinematic GNSS positioning using a multifrequency GNSS receiver is applied to achieve high absolute measurement accuracy. In recent years, low-cost and high-precision single-frequency RTK-GNSS positioning is also available for use in mobile 3D measurement systems. However, although IMUs have improved the price and size of MEMS technology, high-priced IMUs are still required for mobile mapping systems for high relative measurement accuracy.

Mobile 3D measurement systems for surveying are similar to mobile 3D measurement systems for autonomous mobile robots. Simultaneous localization and mapping (SLAM) is a popular approach

for mobile 3D measurement systems for autonomous mobile robots. The SLAM is an algorithm used to simultaneously estimate self-position and maps. The SLAM is roughly classified into real-time SLAM using a Bayesian filter, real-time SLAM with point cloud alignment and optimization (scan matching), and offline SLAM using graphs (graph-based SLAM). The SLAM using a Bayesian filter is a methodology used to fuse prior probabilities and likelihoods stochastically. Extended Kalman filter (EKF) SLAM (Weingarten et al., 2005) and Rao-Blackwellized particle filter (RBPF) SLAM (Murphy, 2000) are popular algorithms used in this methodology. The scan matching consists of two methodologies. In the first methodology, initial positions are used. The iterative closest point (ICP) algorithm (Chen et al., 1992) and normal distributions transform (NDT) algorithm (Biber et al., 2003) are popular algorithms used in this methodology. In the second methodology, global optimization without initial positions is applied. The globally optimal ICP (Go-ICP) algorithm (Yang et al., 2016) is a popular algorithm used in this methodology.

The graph-based SLAM is a methodology used to optimize a graph of self-position and landmark relationships. The graph-based SLAM consists of the front end (sensor-dependent processing) and back end (sensor-independent processing). The front end holds sequential SLAM processing including self-position estimation, loop closure detection, and graph generation. The back end holds graph optimization with graph solvers. Open-source SLAM includes gmapping (RBPF-SLAM) (Grisetti et al., 2007), Hector SLAM (EKF and scan matching using 2D cells) (Kohlbreche et al., 2011), and LiDAR odometry and mapping (LOAM) (point-to-line or point-to-face matching) (Zhang et al., 2014), Velodyne SLAM (point-surface matching and distortion rectification) (Moosmann et al., 2011), and Google Cartographer (sequential SLAM by cell-based scan matching and graph-based batch SLAM processing) (Nüchter et al, 2017).

In this study, we focus on scan matching. Scan matching is an approach used to estimate a rotation matrix and translation vector as the relative rotation and translation of reference point clouds. The main part of scan matching is point cloud alignment between base point clouds and reference point clouds. The rotation matrix and translation vector are estimated with singular value decomposition (SVD) using corresponding points obtained in point cloud matching. The SVD holds the product of an M-by-N orthogonal matrix, N-by-M diagonal matrix, and N-by-N orthogonal matrix. The SVD is often applied for rotation and translation estimation with an ICP algorithm in point cloud matching. Point cloud matching with an ICP algorithm is a methodology used to estimate a rotation matrix and translation vector with outlier rejection by robust estimation such as the random sample consensus (RANSAC). The estimation consists of minimizing of the Euclidean distance between each nearest point among the base and reference data with iterative calculation. However, when sparse point clouds are input, point cloud matching with an ICP algorithm cannot easily determine precise corresponding points because of insufficient point cloud density. Therefore, the matching of the sparse point cloud should be shape-based. Methodologies for higher speed point cloud matching include an input point cloud reduction with uniform sampling or weighted sampling and point cloud matching with an NDT algorithm. Point cloud matching with an NDT algorithm can achieve a higher processing speed than that with an ICP algorithm. The point cloud matching with an NDT algorithm can is processed through the following steps. First, point clouds are assigned into a cell space, such as 2D cell space or 3D voxel space. Next, the average coordinate value is assigned to each cell. Then, the covariance matrix is obtained from the average coordinate values. Afterward, point clouds are represented with a normal distribution using the average coordinate values and the covariance matrix. Finally, matched point clouds are obtained by minimizing the Mahalanobis distance to the normal distribution of the corresponding cell.

Typical issues in scan matching include error accumulation in position estimation, high calculation cost of point cloud matching and optimization, and self-position loss in position estimation failures. In SLAM, error adjustment is generally applied for accumulated errors in position estimation based on a loop closure. The loop closure approach is an error adjustment methodology in SLAM using the same features at the start and end points of the measurement route. Moreover, in SLAM in indoor environments, an error adjustment can be applied with geometric rectification based on the Manhattan World Assumption (a geometric constraint with artificial objects composed of vertical, horizontal, and parallel planes) after scan matching.

The technical issue in scan matching can be simplified from 6 degrees of freedom (DoF) with

rotation angles and position data to 3 DoF with rotation angle when high-precision positioning such as RTK-GNSS is applied. The simplification of scan matching can avoid technical issues in scan matching such as the error accumulation in position estimation. Moreover, the simplification of scan matching can omit the use of IMUs in mobile 3D measurement systems. However, the technical issue of 3 DoF is not easily solved with a combination of positioning data with 2D LiDAR (LiDAR with a single scanning line).
Therefore, we focus on the use of RTK-GNSS positioning and multilayer LiDAR (LiDAR with many scan scanning lines). We aim to develop a registration methodology for point clouds acquired on a road with mobile 3D measurement systems. We also propose a scan matching using geometric constraints that extend the Manhattan World Assumption to road spaces. Through experiments on mobile mapping using multilayer LiDAR mounted on a UAV and cart, we verify that point clouds can be integrated without IMUs. We also verify that our proposed methodology can avoid the error accumulation issue in SLAM.

## 2. METHODOLOGY

Multilayer LiDAR generally holds a wide-angle and high-angular resolution in the horizontal direction (scanning direction) and narrow-angle and low-angular resolution in the vertical direction (between scan rows). When multilayer LiDAR is horizontally mounted onto a mobile platform for road surface measurement, the horizontal cross sections and wide road surface areas can be sufficiently measured. Moreover, the yaw and pitch angles in SLAM processing can be easily estimated. However, compared with the point cloud density in the horizontal cross-sectional direction, that in the vertical direction is sparse. Thus, roll angle estimation becomes difficult because the cross-sectional shape is not clear.
In contrast, when multilayer LiDAR is vertically mounted on a mobile platform for road surface measurement, the cross sections become clear, and roll angle estimation in SLAM can be easily estimated. However, pitch and yaw angle estimations become difficult, because the measurement range of longitudinal sections direction becomes extremely narrow, and shapes in the horizontal cross section direction and road surfaces becomes poor.
Consequently, conventional approaches use two multilayer LiDARs for simultaneous horizontal and vertical scanning (Velas et al., 2019) or rotated multilayer LiDAR for point cloud acquisition in the panoramic range (360 degrees in horizontal and vertical directions) (Sofonia et al., 2019). Both approaches can perform precise point cloud matching in an environment surrounded by random features such as a tunnel, or in an environment surrounded by artificial features such as an indoor environment or streets. However, both approaches require error adjustment with loop closure because of sequential point cloud matching.
Therefore, in our methodology, we avoid the error accumulation issue with global point cloud matching among base and reference point clouds. Models generated with geometric constraints and all scan data are used as base point clouds, and each scan datum is used as reference data. The proposed methodology is a mobile 3D measurement system consisting of a multilayer LiDAR and RTK-GNSS devices. Moreover, the proposed methodology integrates point clouds that measured a rigid and static environment. This work used a carry cart, vehicle, and UAV, as mobile platforms to achieve stable movement along a straight line.
A multilayer LiDAR is mounted on a mobile platform diagonally (forward or backward) with respect to the horizontal plane for uniform point cloud generation in horizontal and vertical directions after point cloud registration. Point cloud acquisition is conducted with the following several requirements. First, the measurement environment requires open sky environments to use GNSS positioning. Second, a one-way measurement along a straight line is applied because loop closure is not required. Third, point cloud acquisition allows several degrees of rotation changing per second by vibration. Before or after 3D measurement, the surface estimation using RANSAC is applied to the acquired point cloud using scan data to estimate offset values consisting of the mounting angles (roll and pitch angles) and height from the road surface of LiDAR.
The coordinate system in processing is defined as follows. First, the center of multilayer LiDAR is used as the origin point, and the average of translation vectors is used as the reference axis. The

translation vector is a vector on the horizontal plane estimated in the local movement, and it is estimated from RTK-GNSS positioning results. The reference axis is the *Y*-axis, the axis orthogonal to the reference axis on the horizontal plane is the *X*-axis, and the remaining axis is the *Z*-axis. The rotation angle around the *Y*-axis is defined as the roll angle, the rotation angle around the *X*-axis is defined as the pitch angle, and the rotation angle around the *Z*-axis is defined as the yaw angle.
The proposed methodology estimates the rotation matrix *R* for point cloud registration without control points. The rotation matrix is estimated based on the following equation with the minimization of residual $\Delta X$ of the corresponding points between the base and reference data.

$$\Delta X = | (R \cdot X_b + t) - X_a | \quad (1)$$

Here, $X_a$ represents the base data, $X_b$ represents the reference data, and $\Delta X$ represents the residuals of corresponding points when $X_b$ is aligned with $X_a$.

The translation vector *t* is determined with RTK-GNSS positioning as a known parameter. The rotation matrix *R* is determined by point cloud matching using RTK-GNSS positioning results and geometric constraints. Point cloud matching consists of roll angle rectification, initial point cloud registration, yaw angle rectification, pitch angle rectification, and yaw angle re-rectification, as shown in Figure 1.

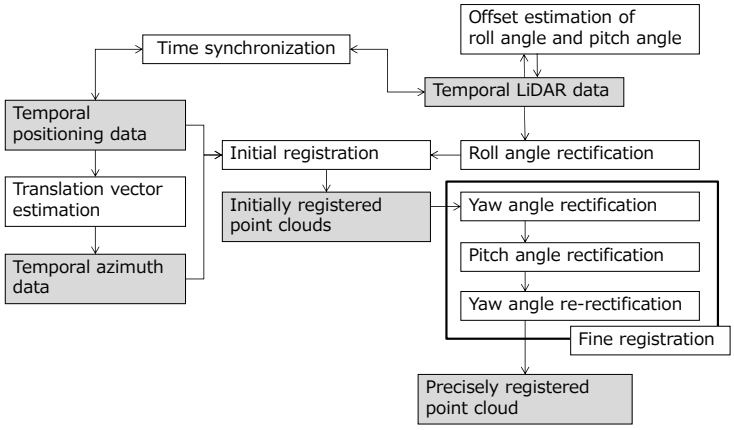


Figure 1. Proposed methodology

## 2.1 Roll angle rectification

A road cross section orthogonal to a road centerline draws an upwardly convex curve because of the drainage on the road surface. The height difference between the road centerline and road edge is small with respect to the road width. The cross slope specified is 1.5-2.0 % in the Japanese road structure ordinance. Therefore, we use a geometric constraint that the road cross-section direction includes horizontal surfaces in each scan datum. Next, point clouds close to LiDAR and in the area of road cross section are selected from each scan datum. The selected point clouds are used for surface estimation by RANSAC. In each scan datum, the estimated surface is rotated on the *Y*-axis, and the horizontal rotation angle is used as the roll angle rectification angle (Figure 2).

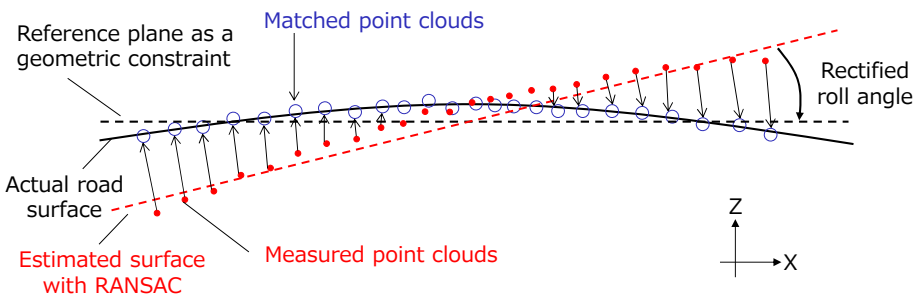


Figure 2. Roll angle rectification

## 2.2 Initial point cloud registration

Initial registration is a process to obtain initially integrated point clouds to rectify the yaw and pitch angles of LiDAR. First, translation vectors are estimated from the time-series positioning data obtained by RTK-GNSS positioning, and the time-series azimuth angle data are estimated. The estimated azimuth angles are used as the yaw angles. Moreover, the offset values of the LiDAR position are used as the roll and pitch angles. Then, each scan datum is rotated around the *Z*-axis, and the rotated scan data are translated with time-series positioning data obtained by RTK-GNSS positioning. All rotated and translated scan data are used as the initially integrated point clouds.

## 2.3 Yaw angle rectification

The yaw angle rectification consists of linear segment extraction from the initially registered point clouds and scan data matching with the extracted linear segments. First, point clouds within higher positions than road surfaces are extracted from initially registered point clouds using the offset values of the LiDAR position. Next, the extracted point clouds are projected into raster data with arbitrary spatial resolution, and linear segments, such as guardrails, road edges, and electric cables, are extracted in the projected point clouds by Hough transformation (Figure 3). Afterward, parallel representative line segments are selected from the extracted linear segments to be used as guardrails or road edges. These line segments are used as base data, and each scan datum after the initial registration is used as reference data. Then, scan matching is performed with *Z*-axis rotation to estimate the rectification yaw angle for each scan datum (Figure 4).

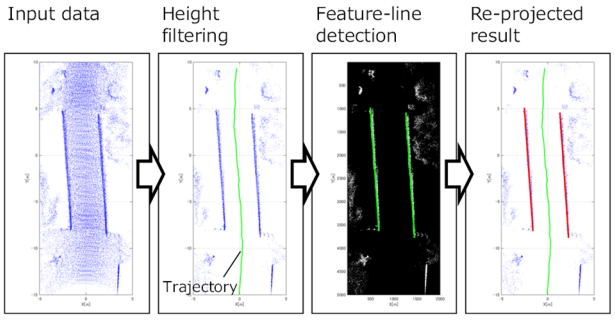


Figure 3. Straight line extraction

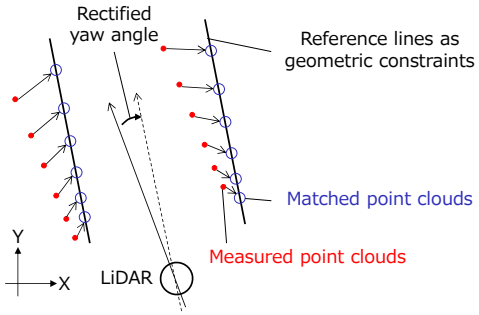


Figure 4. Rectification of yaw angle

## 2.4 Pitch angle rectification

In the pitch angle rectification, point clouds and extracted parallel line segments are first rotated and translated to adjust along the *X*- or *Y*-axis of processing space for higher processing in the re-rectification of pitch and yaw angles (Figure 5). Next, after the yaw angle rectification, the point clouds along the center of parallel line segments are automatically selected to estimate the longitudinal section line. The longitudinal section line is used as the base data, and each scan datum rectified with yaw angles is used as the reference data. Then, scan matching is performed with *X*-axis rotation to estimate the rectification pitch angle for each scan datum (Figure 6).

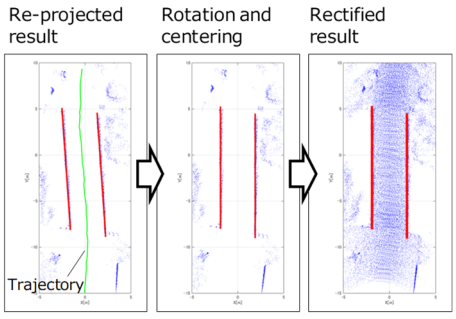


Figure 5. Preprocessing of pitch angle

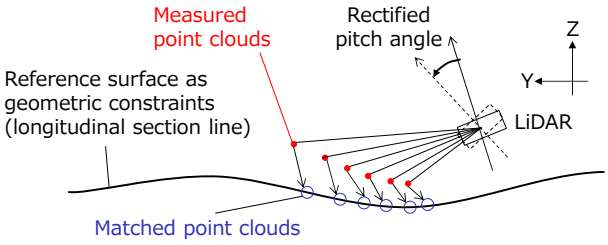


Figure 6. Pitch angle rectification

### 2.5 Yaw angle re-rectification

Each scan datum after the pitch angle rectification is further rectified with *Z*-axis rotation based on point cloud matching, and the rectified results are used as yaw angles of each scan datum. Although the yaw angle re-rectification follows the same methodology as the first yaw angle rectification, the input point clouds are different from those at the first rectification (point clouds after pitch angle rectification are input in the re-rectification). Moreover, line segments after the re-registration can be used as more precise base data for point cloud matching, because line segments are extracted from integrated point clouds with the rectification of each scan datum.

## 3. EXPERIMENTS

In our experiment, we used a multilayer LiDAR (VLP-16, Velodyne) with GPS antenna for timing (Figure 7) and a single-frequency RTK-GNSS receiver and antenna (C94-M8P-4, u-blox) (Figure 8). Single-frequency RTK-GNSS positioning is position data acquisition with single-frequency GNSS receivers that enables multi-GNSS positioning by combining GPS, GLONASS, BeiDou, and QZSS to perform RTK-GNSS positioning. In our experiments, a combination of GPS, BeiDou, and QZSS was applied using u-center v19.06 (u-blox). A GPS antenna was connected to LiDAR, and GPS time was recorded along with laser scanning using Velodyne v3.5.0 (Velodyne). The GPS time assigned to the LiDAR data was used to synchronize the time between the laser scanning data and the RTK-GNSS positioning data with a 1-Hz sampling rate. Besides, a single-frequency RTK-GNSS reference station was installed near the measured objects. We installed the reference station consisting of a single-frequency RTK-GNSS receiver (C94-M8P, u-blox) and an antenna (Zephyr Geodetic 2, Trimble), and the reference station was connected wirelessly to the receiver on the mobile platform using u-center v19.06 (u-blox). In single-frequency RTK-GNSS positioning, a Fix status was obtained after approximately 15 minutes of initialization, and positioning accuracy was several centimeters under open sky environments with a continuous Fix status until the end of laser scanning.


| | |
|---|---|
| Distance measurement accuracy | 3 cm |
| Angular resolution (horizontal) | 0.25 deg |
| Angular resolution (vertical) | 2.0 deg |
| Measurement range (horizontal) | 360 deg |
| Measurement range (vertical) | ±15 deg |
| Sampling rate | 10 Hz |

Figure 7. VLP-16 (Velodyne)

| | |
|---|---|
| Captureable satellites | GPS L1 C/A, GLONASS L1OF, BeiDou B1I |
| Number of channels | 72 |
| Time pulse signal accuracy | 30 ns (RMS), 60 ns (99 %) |
| Communication frequency between rovers and reference station | 920 MHz |

Figure 8. C94-M8P-4 (u-blox)

We conducted two types of experiments. The first experiment was a preliminary experiment on initial point cloud registration using UAV without the influence of positioning environments. The second experiment was an experiment on point cloud registration using land-based measurement under the influence of the positioning environment. In the preliminary experiment, UAV (E-695MP, EAMS ROBOTICS) was used, and LiDAR was mounted on a gimbal installed with a forward direction of 20 degrees from the vertical axis (Figure 9). After the initialization to obtain the Fix status for RTK-GNSS positioning, LiDAR and position data were acquired along the longitudinal direction of a river with one-way measurement.

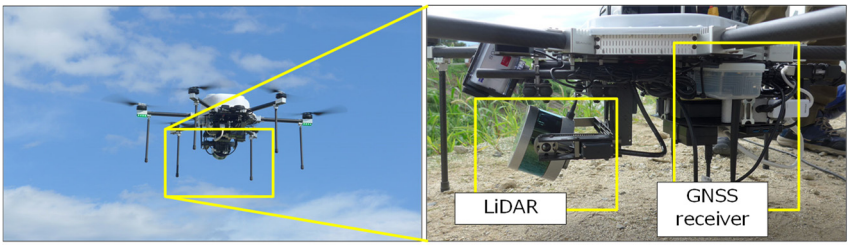


Figure 9. Mobile 3D measurement system (UAV)

In the experiment using a cart, LiDAR was mounted on the cart in the downward direction at approximately 30 degrees and a height of 1 m from the road surface (Figure 10). The single-frequency RTK-GNSS antenna was mounted on the cart at a position of 0.22 m in the horizontal direction and a height of 0.35 m from the LiDAR. After the initialization to obtain the Fix status for RTK-GNSS positioning, LiDAR and position data were acquired from the cart pulled at a speed of 1 km/h along the centerline of the road. A small road bridge (12.5 m length and 4.2 m width) was selected as a measured object. Markers as verification points were installed at three positions along the centerline of the road and three positions on each side of the road. The center position of each marker was measured by a nonprism total station, and global coordinate values were obtained using a public reference point (Figure 11). We acquired 527 scans and 8,521,697 points, and we selected point clouds below the LiDAR position and within a distance of 5 m from the LiDAR. The search range in the pitch angle was 2 degrees, and the search range in the yaw angle was 10 degrees. The spatial resolution of the raster data used in Hough transformation in the yaw angle rectification was 0.005 m. We compared scan matching processing using ICP and NDT algorithms (conventional algorithms) with our proposed methodology.

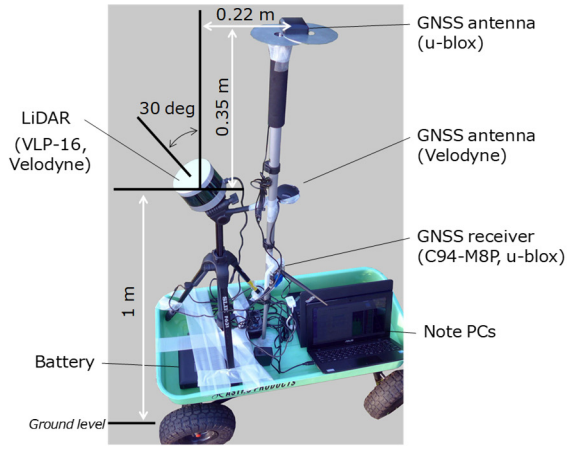


Figure 10. Mobile 3D measurement system (pull-type mobile mapping system)

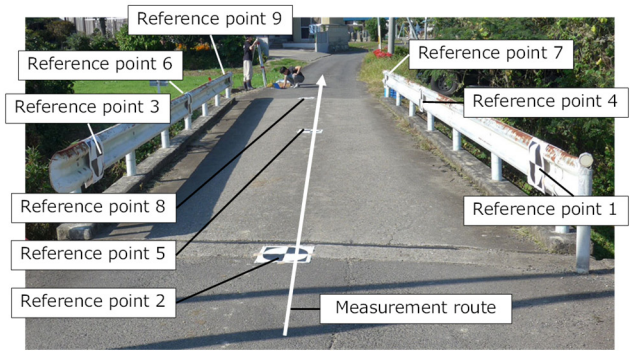


Figure 11. Verification point layout

## 4. RESULTS

Figure 12 shows the preliminary experimental results of the initial point cloud registration to compare our proposed methodology with the scan matching processing using an ICP algorithm.

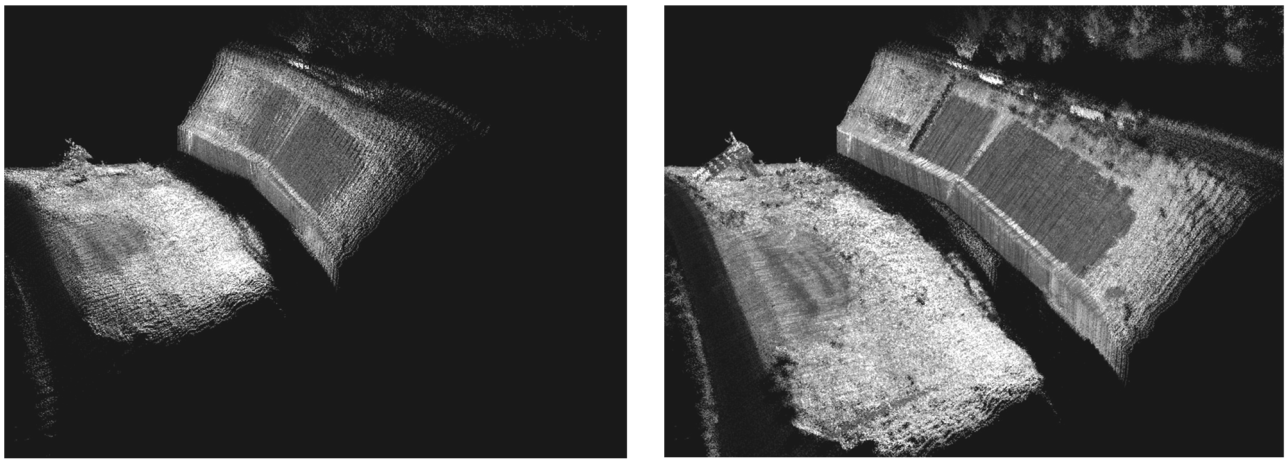

Figure 12. Preliminary experiment results on initial point cloud registration using UAV LiDAR data (left: scan matching processing using an ICP algorithm, and right: proposed methodology)

Figure 13 shows the results of the scan matching with ICP, NDT, and proposed algorithms obtained in mobile 3D measurement using the cart. The processing time for each methodology was ICP registration: 364.69 seconds, NDT registration: 809.61 seconds, and proposed methodology: 400.64 seconds.

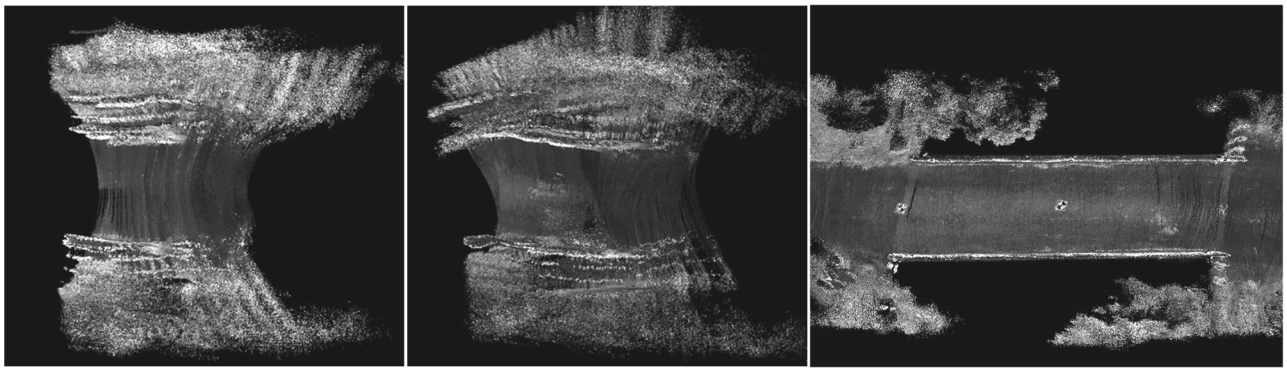

Figure 13. Point cloud registration results using a pull-type mobile mapping system (left: scan matching processing with an ICP algorithm, center: scan matching processing with a NDT algorithm, and right: proposed methodology)

We compared the results of the conventional and our proposed methodology. As shown in Figures 12 and 13, conventional approaches failed to register point clouds. In contrast, we qualitatively evaluated that our proposed methodology sufficiently registered point clouds. The reason for failure in the point cloud registration with the conventional approaches is that the point cloud of each scan datum is too sparse among each scanning line to find corresponding points, even if the error values are small enough between the base and reference data, as shown in Figure 14. In contrast, in our proposed methodology, point clouds corresponded easily between the base and reference data, because the base data are dense point clouds.

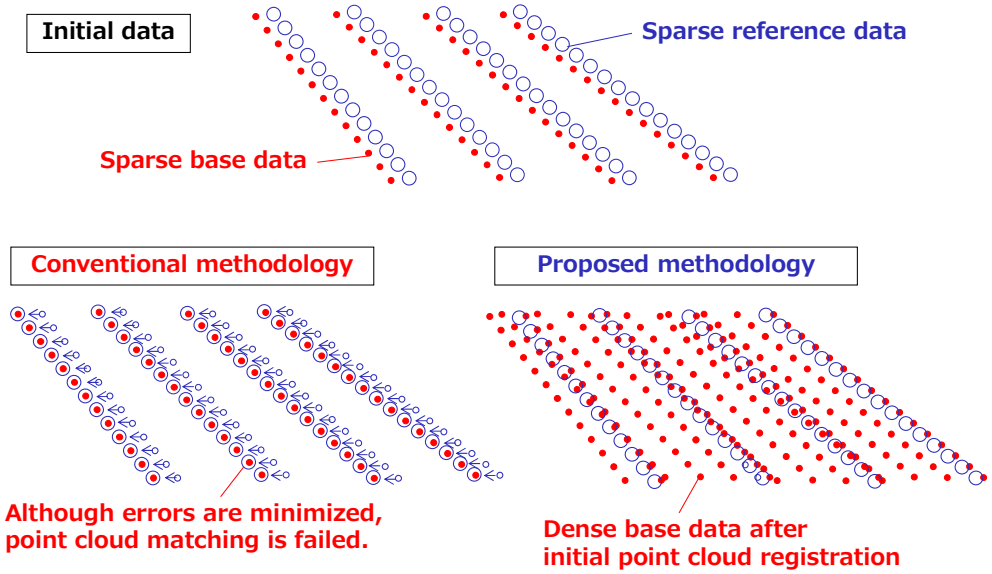


Figure 14. Point matching using sparse point clouds as input data

Figure 15 shows the initial and fine registration results. The initially registered point clouds were thick at thin guardrail surfaces, as shown in the left images of Figure 15. In contrast, point cloud representation was improved after fine registration, as shown in the right images of Figure 15. Moreover, unclear markers in the initially registered point clouds (left images in Figure 15) become clear markers in the fine registered point clouds (right images in Figure 15).

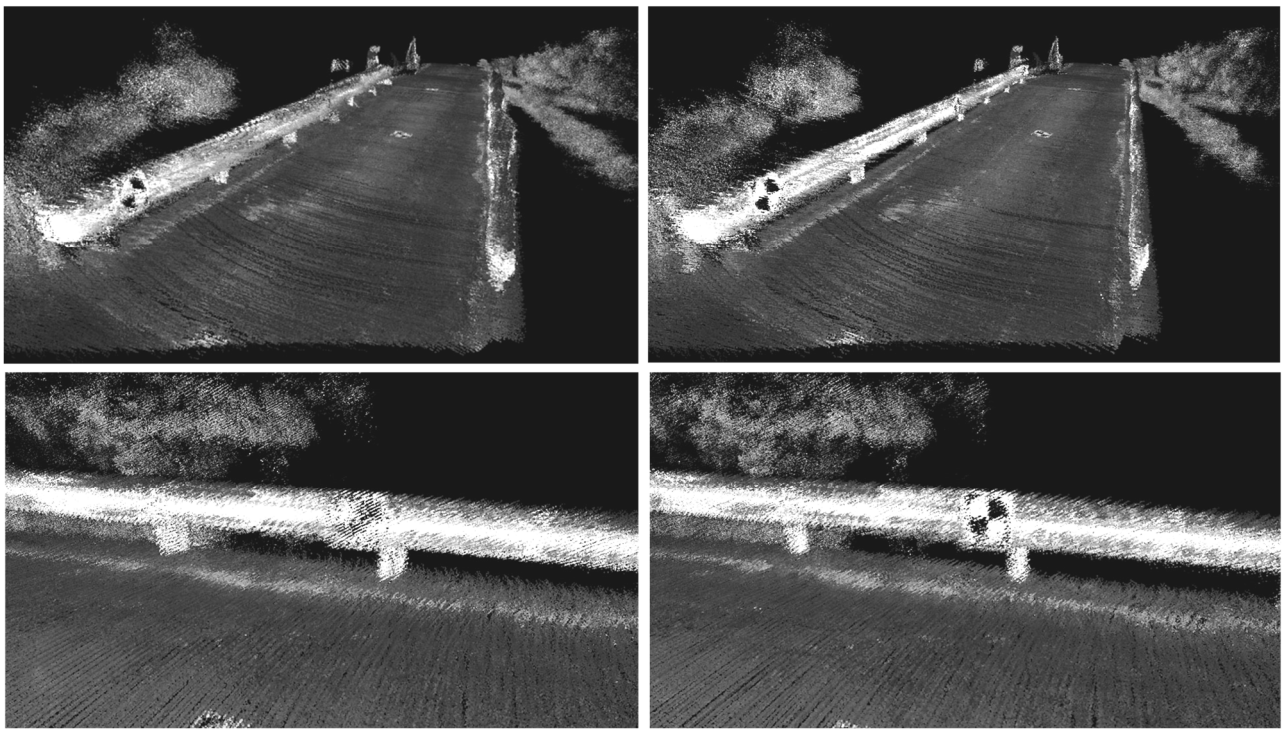

Figure 15. Registered point clouds (left: initial registration result, and right: fine registration result)

Furthermore, the registration accuracy was verified using the verification points (markers). The point clouds were registered with the ICP algorithm using markers 1, 3, 7, and 9. Then, the registration accuracy was evaluated by the registration errors using markers 2, 4, 5, 6, and 8. The relative accuracy was X = 0.082 [m], Y = 0.036 [m], and Z = 0.019 [m] (RMSE); and the accuracy in the 3D direction was 0.092 [m] (RMSE). We confirmed that point clouds were registered well because the distance measurement accuracy of VLP-16 is approximately 3 cm.

In the preliminary experiment of single-frequency RTK-GNSS positioning to acquire observation data for 1 hour at a fixed point, the relative accuracy was X = 0.0099 [m], Y = 0.0434 [m], and Z = 0.0422 [m] (RMSE). Moreover, the accuracy in the 3D direction was 0.061 [m] (RMSE). The accuracy of the mobile 3D measurement system was calculated as 0.068 [m] (RMSE) based on the error propagation using catalog values of the accuracy of LiDAR distance measurement and RTK-GNSS positioning. Thus, the acquired data are matched with the theoretical values.

Additionally, we evaluated the registration error with other combinations of markers. When point clouds were registered with the ICP algorithm using markers 4, 6, 7, and 9 as reference targets, the relative error value of markers 5 and 8 as verification targets was X = 0.063 [m], Y = 0.030 [m], and Z = 0.017 [m] (RMSE). The improved accuracy of registration indicates the possibility that the length of line segments at the start or end points of the bridge was too short to apply for the line segment matching (the amount of reference data is insufficient) in the yaw angle rectification and re-rectification.

In our experiment, because the road bridge was selected as a measured object, the guardrails were extracted as linear features in the yaw angle rectification. Our methodology can be applied to other objects when the objects contain linear features such as wall surfaces near the trajectory line on the horizontal plane. Moreover, when the model fitting methodology is applied with known models such as curved features, the yaw angle can be rectified at curve areas.

## 5. CONCLUSION

In this paper, we focused on the use of RTK-GNSS positioning and multilayer LiDAR to improve point cloud registration in SLAM. We proposed a registration methodology for point clouds acquired using mobile 3D measurement systems with the extended Manhattan World Assumption as geometric constraints. Through experiments on mobile mapping using multilayer LiDAR mounted on a UAV and cart, we verified that point clouds can be integrated without IMUs. We also verified that our proposed methodology can avoid error accumulation issues in SLAM.

**REFERENCES**


Weingarten, J., Siegwart, R., 2005. EKF-based 3D SLAM for Structured Environment Reconstruction, Proc. IEEE/RSJ International Conference on Intelligent Robots and System, pp.2089-2094.

Murphy, K., 2000, Bayesian Map Learning in Dynamic Environments, Advances in Neural Information Processing Systems 12, pp.1015-1021.

Chen, Y., Medioni, G., 1992, Object Modelling by Registration of Multiple Range Images, Image Vision Computing. Butterworth-Heinemann, Vol. 10, Issue 3, pp. 145-155.

Biber, P., Straßer, W., 2003, The Normal Distributions Transform: A New Approach to Laser Scan Matching, Proceedings of IEEE/RSJ International Conference on Intelligent Robots and Systems (IROS), Vol. 3, pp. 2743–2748.

Yang, J., Li, H., Campbell, D., Jia, Y., 2016, Go-ICP: A Globally Optimal Solution to 3D ICP Point-Set Registration, IEEE Transactions on Pattern Analysis and Machine Intelligence, 14 pages.

Grisetti, G., Stachniss, C., Burgard, W., 2007, Improved Techniques for Grid Mapping with Rao-Blackwellized Particle Filters, IEEE Transactions on Robotics 23, pp.34-46.

Kohlbreche, S., Stryk, O., Meyer., J, Klingauf, U,. 2011, A Flexible and Scalable SLAM System with Full 3D Motion Estimation, IEEE International Symposium on Safety, Security, and Rescue Robotics, pp.155-160.

Zhang, J., Singh, S., 2014, LOAM: Lidar Odometry and Mapping in Real-time, Robotics: Science and Systems, 9 pages.

Moosmann, F., Stiller, C., 2011, Velodyne SLAM, 2011 IEEE Intelligent Vehicles Symposium (IV), pp.393-398.

Nüchter, A., Bleier, M., Schauer, J., Janotta, P., 2017, Improving Google's Cartographer 3D Mapping by Continuous-Time SLAM, The International Archives of the Photogrammetry, Remote Sensing and Spatial Information Sciences, Volume XLII-2/W3, pp.543-549.

Velas, M., Spanel, M., Sleziak, T., Habrovec, J., Herout, A., 2019, Indoor and Outdoor Backpack Mapping with Calibrated Pair of Velodyne LiDARs, Sensors, vol. 2019, no. 18, pp. 1-34.

Sofonia, J., Phinn, S., Roel fsema, C., Kendoul, F., Rist, Y., 2019, Modelling the effects of fundamental UAV flight parameters on LiDAR point clouds to facilitate objectives-based planning, ISPRS Journal of Photogrammetry and Remote Sensing, Vol.149, Pages 105-118.